Article:
Yu, Y., Horoshenkov, K.V., Sailor, G. et al. (2025) Sparse representation for artefact/defect localization with an acoustic array on a mobile pipe inspection robot. Applied Acoustics, 231. 110545. ISSN: 0003-682X

https://doi.org/10.1016/j.apacoust.2025.110545

Sparse representation for artefact/defect localization with an acoustic array on a mobile pipe inspection robot

Yicheng Yu [a,*], Kirill V. Horoshenkov [a] , Gavin Sailor[b] and Simon Tait[b]

[a] Department of Mechanical Engineering, University of Sheffield, Mappin Street, Sheffield S1 3JD, UK.

[b] Department of Civil and Structural Engineering, University of Sheffield, Sheffield S1 3JD, UK

* Corresponding author. E-mail address: Yicheng.Yu@sheffield.ac.uk

Key words: mobile compensation, pipe, sparse representation, direction estimation, microphone array

Abstract

Autonomous robots equipped with long-range acoustic sensing are revolutionizing the inspection of extensive sewer networks by accurately detecting and mapping artefacts and defects that could cause a pipe operational failure. This study introduces a frequency domain Sparse Representation (SR) method for identifying artefacts and defects using a circular microphone array mounted on a mobile inspection robot. The circular array enhances the precision of localization by extracting plane wave modes at frequencies above the pipe's first cut-off frequency. The proposed mobile compensation algorithm can separate overlapping echoes with less than 0.5% error of the sensing distance, given sufficient overlap in acoustic wavelengths. It also compensates for phase shifts and reduces noise from a moving robot, enabling accurate estimation of defect direction and distance amid overlapping acoustic echoes. The paper evaluates the algorithm's effectiveness concerning signal excitation duration, aiming

to enhance acoustic inspection techniques for continuously moving autonomous robots in buried pipes.

1. Introduction

Buried pipe networks are used to transport a variety of fluids. Such networks are often complex with a range of artefacts, such as lateral connections, valves and terminations. The pipes within these networks can suffer damage during installation and also deteriorate with time, and it is necessary to understand their physical condition as operational defects such as leaks and blockages can cause significant hydraulic performance, safety and environmental hazards. For example, in the UK alone there are over 600,000 km of sewer pipes and 350,000 km of clean water pipes and in the EU there are more than 4.3 million km of water supply pipes, and more than 3 million km of wastewater collection pipes [1]. Most of these pipes are round and made of concrete or clay. Given their function and size these pipe networks require reliable and low-cost inspection techniques for artefact and defect detection. In 2017, it was estimated that there were approximately 300,000 blockages in sewers each year in the UK, resulting in around £100M of consequential costs [2]. Currently, there is strong regulatory pressure to develop more efficient techniques to locate blockages and to map system artefacts, due to their heavier usage resulting from population growth, increasing demand for water and climate change [3].

Autonomous robotic sensing systems [4] working in buried pipes for condition monitoring and fault detection offer the opportunity to capitalise on recent advances in acoustic and ultrasonic sensing techniques. Acoustic methods have been investigated for blockage detection and condition assessment in sewage [5] and water [6] pipes, and have significant practical advantages over current Closed-Circuit Television (CCTV) inspections due to their much further detection range, less power consumption and less computation cost. This review suggests that there is a lack of acoustics inspection methods that can be applied from a mobile robot to localise and classify in-pipe defects. Acoustically reflective artefacts/defects including

lateral connections, in-pipe blockages and physical damage can be localized remotely with respect to the robot position using the time delay of acoustic echoes measured with a microphone [7]. Recently, a circular microphone array was used to extend the acoustic frequency range on a robotic platform to detect, localize and classify more reliably blockages or lateral connections in pipes using Sparse Representation (SR) and Support Vector Machine (SVM) methods [8, 9]. However, this method only worked while the inspection robot was static. In order to determine the direction of the echo arrival, acoustic measurements were implemented sequentially at several discrete robot positions with a 0.2m separation [8]. This approach limits the operational efficiency of condition detection using an inspection robot, increases the complexity of the algorithm for robotic autonomous control and increases significantly the time required for robot to traverse the inspected length of the pipe.

Microphone array analysis has also been used with an in-duct wall mounted array [10] or out-duct array [11] for sound source localization in ducts in the application of noise characterization in aeroengineering. These methods use beamforming technology and deconvolution approaches to passively localize the noise source (particularly near-field point source, e.g. [10] in ducts. Different from the noise characterization, this paper is focusing on the localization of pipe conditions at a long range, including blockages, lateral connections and pipe ends/direction changes at chambers. Passive beamforming has also been used for defect localization in pipeline systems such as the identification of leaks in pressurised water pipes [12, 13]. This paper uses an active sensing method with a collocated source and microphone array deployed on a continuously moving robot to inspect pipes within a network. Active acoustic sensing by the moving robot can also enhance its capabilities in localization and mapping (Refs. [14, 9, 8]), as well as potential long-range acoustic communication between the robots in the pipe network (Refs. [15, 16, 17]).

This paper proposes a frequency domain algorithm to enable the inspection robot to measure the acoustic response of the pipe, and hence artefacts and defects, whilst the robot is moving. This inspection capability is achieved with an acoustic array and through the compensation of the phase shift induced by the mobile robot. Different from the time domain algorithm [8] with deconvolution directly applied to estimate the impulse response for robotic localization, the frequency domain method proposed in this paper uses a Sparse Representation (SR) method that compensates for the inspection robot's velocity. It also significantly improves the precision of localization and separates the overlapping acoustic echoes (when the artefact/defect separation is larger than the minimum wavelength of excitation for a static robot).

The structure of this paper is organised as follows. Section 2 discusses the theoretical framework of the SR method to estimate the location of the artefacts/defects in a pipe with a mobile robot equipped with a speaker and microphone array. The experimental validation setup is presented in Section 3 with the robotic sensing system and testing environment of pipe network. The estimation results using the Least Square (LS) and SR are compared in Sections 4.1 and 4.2 for a static and moving robots, respectively. The effects of the chirp duration and adopted frequency range on the accuracy of localization are discussed in Section 4.2.1 and Section 4.2.2, respectively.

2. Theory

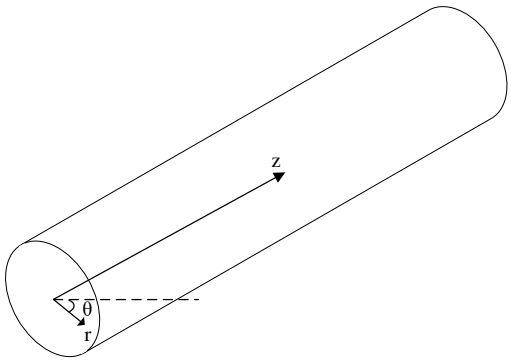

Figure 1. Coordinates system used in a "cylindrical" pipe.

In the frequency domain the acoustic field in a cylindrical pipe can be expressed as the superposition of modes as suggested by Morse and Ingard [18]:

$$p(r,\theta,z,\omega) = \sum A_{mn}\varphi_{mn}(r,\theta)e^{-\mathrm{i}\gamma_{mn}z} \quad (1)$$

where ω is the angular frequency, m and n are the mode indices, φ_{mn} is the mode shape function of the cross-section, A_{mn} is the modal amplitude. Pipe materials for UK sewers are mainly concrete, clay or plastic with a much higher characteristic acoustic impedance than of the air. Therefore, the pipe surface can be assumed as rigid for an air filled pipe. The z-axis wavenumber in Eq. (1) is given by [18]:

$$\gamma_{mn} = \sqrt{k_0^2 - k_{mn}^2} \quad (2)$$

where k_0 is the wavenumber in a free space ($k_0 = \omega/c_0$, c_0 is sound speed in air). For a partially filled pipe, the non-axisymmetric acoustic modes may split and introduce complexity for the post-processing of acoustic data [19]. This paper ignores the effects of partially filled water pipe. Furthermore, different pipe materials may also affect the sound propagation, e.g. roughness [20] in concrete pipes which is not considered in this paper. The mode shapes,φ_{mn}, and wavenumbers, k_{mn}, in Eqs. (1) and (2) for partially filled pipes, non-round pipes or pipe with wall roughness can be predicted analytically, e.g. [19,20], or via a numerical simulation. Eq. (2) predicts the wavenumber at which acoustic modes at different frequencies propagate in the pipe. It is clear that γ_{mn} is frequency dependent, i.e., the acoustic propagation of these modes (except in the case of plane wave when $k_{00} = 0$) is dispersive. If the free field wavenumber k_0 is larger than the eigen-number k_{mn}, or the frequency is above the corresponding eigen-frequency, $f_{mn} = k_{mn}c_0/(2\pi)$, then a particular acoustic mode can propagate along the pipe with relatively little attenuation at a phase velocity that is dispersive. Figure 2(a) shows schematically the angular and radial dependence of the first four mode

shapes in a cylindrical pipe. In Figure 2 the plus or minus sign corresponds to the sign of the modal shape, φ_{mn}, takes for a given values of θ and r in Eq. (1).

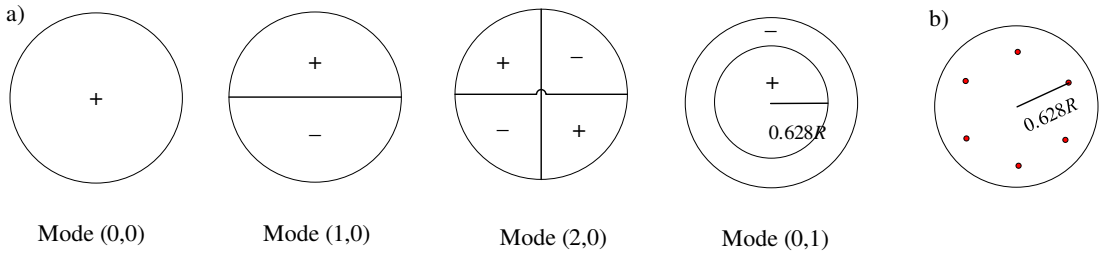

Figure 2. (a) An illustration of the behaviour of the first 4 modal shapes in a cylindrical pipe; (b) position of the microphone array for the plane wave reconstruction above the first cut-on frequency [8].

Recently it was proposed to use a six circular microphone array to filter out the plane wave mode in the frequency range well above the first cut-on frequency in a round pipe [8]. The location of these microphones in the array was proposed to be along the $0.628R$ circumference, see Figure 2(b) to mute the unwanted axisymmetric mode (f_{01} = 2789 Hz for a 150 mm dry, air-filled pipe). In this case an optimal cancellation of the first two non-axisymmetric modes (1,0), (2,0) can be achieved by averaging the measured acoustic response to extract the plane wave only over a relatively broad frequency range of k_0R<5.5 (e.g. below 4 kHz for a 150mm pipe). This paper uses the same setup for the microphone array where only the plane wave is extracted and analysed within the same frequency range, that is below 4 kHz in a 150 mm air-filled pipe.

For an acoustic sensing system with the static excitation and receiver points co-located in the pipe, the acoustic response at the plane wave mode ($\gamma_{mn} = k_0$ in Eq. (1)) can be expressed as:

$$p(z_0, \omega) = \sum_{q=0}^{Q} A_{00}(\omega) e^{-2ik_0|z_q - z_0|} s(z_q) + n(\omega) \qquad (3)$$

where z_0 is the coordinate of the sensor array installed on an inspection robot, z_q is the discrete axial coordinates, z_Q is the maximum estimated distance. The spatial resolution of this method is defined as $\Delta z_q = c_0 \Delta t$, and is dependent on the time step, $\Delta t = 1/f_s$ in the sampling of the reflected acoustic signal. The time series $t_{q'} = q' \Delta t$ is the q' th time sampling interval, where $q' = |q|$, and f_s is the sampling frequency used for data acquisition.

In Eq. (3) $A_{00}(\omega)$ is the spectrum of the excitation signal in the plane wave mode (usually a chirp [8]). $s(z_q)$ is the amplitude of the reflection from the artefact/defect located at the position z_q, which can be understood as the reflection coefficients, but modulated by the frequency response of the speaker. The amplitude of the source is also included in the vector $\boldsymbol{s}$. When there are no artefacts/defects at z_q, $s(z_q)$ is equal to zero. Therefore, it is expected that the artefacts/defects amplitude $\boldsymbol{s} = \{s_1, \ldots, s_Q\}$ is a sparse vector with many zeroes due to the sparse nature of the artefacts/defects found in buried pipe networks [8]. $n(\omega)$ denotes residue errors between the measured sound pressure and the prediction model. Note that the phase lag term in the exponent $e^{-2ik_0|z_q - z_0|}$ uses twice the distance between the sensor array and the locations of the artefacts/defects, because the wave propagates from the robot to the artefacts/defects and is then reflected back. As the acoustic sensing system is mounted on a continuously moving robot, the phase lag in the exponent in Eq. (3) due to the moving robot should be compensated for. To the best of our knowledge this concept has not been tested in a pipe environment where the acoustic field is strongly multimodal.

A rigid or open termination at a pipe end can be present in the front of or behind a moving robot as shown in Figure 3. Therefore, the wavenumber in Eq. (5) can take either the positive or negative sign depending upon the direction with respect to the sensors' alignment. It should be possible to identify the direction of the received acoustic echoes from the artefacts/defects with respect to the sign of the velocity at which the inspection robot is moving. Assuming z_0=0,

$\boldsymbol{s}$ can be written as a vector of positive or negative coordinates. For an artefact/defect at a negative coordinate behind the robot the reflected acoustic wave propagates in the positive direction so that the wavenumber in Eq. (5) is positive. For an artefact/defect located in the positive direction in front of the inspection robot, the wavenumber should be negative (see Figure 3). Eq. (5) suggests that it is the difference between the positions of the moving robot, z_0, and artefact, z_q, is of importance rather than their absolute coordinates. In this way the phase compensation to account for the moving robot can be written as:

$$p(z_0, \omega) = \sum_{q=-Q}^{Q} A_{00}(\omega) e^{-2\mathrm{i}|k_0 z_q| - 2\mathrm{sgn}(z_q)[\mathrm{i}k_0 v_r t_r(\omega)]} s(z_q) + n(\omega) \qquad (4)$$

where v_r is the velocity of the robot, $\mathrm{sgn}(\cdot)$ is the sign function, t_r is the time lag of the excitation. Note that the velocity of the in-pipe robot is always much smaller than the speed of sound (e.g. $v_r = 0.1$ m/s $\ll c_0$). Hence, Doppler shift is negligible here for practical robot speeds. If a linear chirp (sinusoidal sweep) signal is used as the excitation, then the time lag from the inspection robot can be expressed analytically as:

$$t_r(\omega) = T(\omega - \omega_1)/(\omega_2 - \omega_1) \qquad (5)$$

where ω_1 and ω_2 are the instantaneous frequency at the beginning and end of the chirp, respectively, and T is the chirp duration. An alternative excitation signal can be used to achieve a similar algorithm efficiency as long as it delivers sufficient acoustic energy across the specified frequency range.

Again, the velocity for the phase compensation term ($e^{-2\mathrm{sgn}(z_q)[\mathrm{i}k_0 v_r t_r(\omega)]}$) is twice of the robot's velocity, v_r, due to distance of wave propagation between the robot and the artefacts/defects and its return. Note that the parameters of acoustic excitation emitted from the moving robot are presented in Eq. (4) by terms $A_{00}(\omega)$ and $s(z_q)$, where the former corresponds to the spectral amplitude, and the latter corresponds to the spatial amplitude. The

spatial amplitude of acoustic excitation covers twice the distance from the moving robot with *T* chirp duration, due to twice of the robot velocity v_r being used for the phase compensation. This velocity can be understood as the real and imaginary source moving towards each other, resulting in a relative velocity that is twice as pronounced as the robot velocity. This will be discussed along with detailed experimental results presented in Section 4.

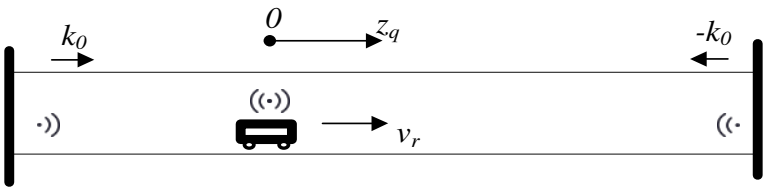

Figure 3. An illustration of a moving inspection robot in a pipe with reflective ends.

In order to estimate the location of the artefacts/defects, Eq. (4) can be solved as an acoustic inverse problem, which can be written as matrices in the discrete frequency domain:

$$\boldsymbol{p} = \boldsymbol{hs} + \boldsymbol{n} \rightarrow \begin{Bmatrix} p_1 \\ p_2 \\ \vdots \\ p_L \end{Bmatrix} = \begin{bmatrix} h_{1,-Q} & h_{1,1-Q} & \cdots & h_{1,Q} \\ h_{2,-Q} & h_{2,1-Q} & \cdots & h_{2,Q} \\ \vdots & \vdots & \ddots & \vdots \\ h_{L,-Q} & h_{L,1-Q} & \cdots & h_{L,Q} \end{bmatrix} \begin{Bmatrix} s_{-Q} \\ s_{1-Q} \\ \vdots \\ s_Q \end{Bmatrix} + \begin{Bmatrix} n_1 \\ n_2 \\ \vdots \\ n_L \end{Bmatrix} \tag{6}$$

where $h_{lq} = A_{00}(l\Delta f)e^{-2\mathrm{i}|k_0(l\Delta f)qc_0\Delta t|-2\mathrm{sgn}(q)[\mathrm{i}k_0(l\Delta f)v_r t_r(l\Delta f)]}$, Δf is the frequency domain resolution of the discrete Fourier transform used to calculate the acoustic response spectrum in Eq. (1), *l* and *q* are the indices of the frequency and distance points, respectively, *L* and $2Q$ are the total numbers of the frequency and distance points, respectively.

Particularly for a static robot, the elements of the transfer matrix h_{lq} are equal to $h_{l,-q}$. The estimated artefact's spatial amplitudes s_q are also equal to s_{-q}. Hence, Eq. (6) with $2Q$ can be reduced to a smaller dimension and rewritten as:

$$\boldsymbol{p} = \boldsymbol{hs} + \boldsymbol{n} \rightarrow \begin{Bmatrix} p_1 \\ p_2 \\ \vdots \\ p_L \end{Bmatrix} = \begin{bmatrix} h_{1,0} & h_{1,1} & \dots & h_{1,Q} \\ h_{2,0} & h_{2,1} & \dots & h_{2,Q} \\ \vdots & \vdots & \ddots & \vdots \\ h_{L,0} & h_{L,1} & \dots & h_{L,Q} \end{bmatrix} \begin{Bmatrix} s_0 \\ s_1 \\ \vdots \\ s_Q \end{Bmatrix} + \begin{Bmatrix} n_1 \\ n_2 \\ \vdots \\ n_L \end{Bmatrix} \tag{7}$$

where $h_{lq} = A_{00}(l\Delta f)e^{-2\mathrm{i}|k_0(l\Delta f)qc_0\Delta t|}$. The direction of the acoustic echo from an artefact/defect is impossible to determine using the Fourier transform of the time series for the acoustic response recorded on a static robot because of the missing term $-2\mathrm{sgn}(q)[\mathrm{i}k_0(l\Delta f)v_r t_r(l\Delta f)]$ in Eq. (9). Therefore, only the positive coordinate toward the artefact/defect can be recovered.

It is assumed that acoustic artifacts possess a spatially limited extent, which ensures that the vector $\boldsymbol{s}$ exhibits significant sparsity. This sparsity, characterized by features such as blockages, junctions, and pipe end, is typical in drainage pipes or sewer networks. Previous studies (Ref. [14, 8, 9]) have demonstrated that the sparsity of the impulse response within these pipes is detectable in both the time and wavelet domains. Moreover, as discussed in Ref. [8, 9], employing the SR effectively diminishes background noise and reduces high-order modal components of the impulse response, without cancelling the acoustic signatures of the artifacts/defects. Similarly, this paper utilizes the sparsity observed in the frequency domain of the artifact's/defect's amplitude $\boldsymbol{s}$, as delineated in Eq. (7).

The sparsest solution $\hat{\boldsymbol{s}}$ should satisfy the following optimization problem [21]:

$$\hat{\boldsymbol{s}} = \arg\min_{\boldsymbol{s}} \|\boldsymbol{s}\|_0 \text{ subject to } \boldsymbol{hs} - \boldsymbol{p} = 0 \tag{8}$$

where $\|.\|_0$ denotes the ℓ_0 pseudo-norm, which is the number of the non-zero components of the vector. This is also referred to as the cardinality of $\boldsymbol{s}$ [21]. The optimization problem in Eq. (8) is non-convex and its solution is usually found by using a brute-force search [21] which can be computationally expensive. Fortunately, it is possible to relax the optimization in Eq. (8) to a convex ℓ_1-minimization [21]:

$$\hat{\boldsymbol{s}} = \arg\min_{\boldsymbol{s}} \|\boldsymbol{s}\|_1 \text{ subject to } \boldsymbol{h}\boldsymbol{s} - \boldsymbol{p} = 0 \quad (9)$$

where $\|.\|_1$ denotes the l_1-norm, which describes the sum of absolute values of the vector.

A related convex optimization problem is the following:

$$\hat{\boldsymbol{s}} = \arg\min_{\boldsymbol{s}} \{ \|\boldsymbol{h}\boldsymbol{s} - \boldsymbol{p}\|_2^2 + \lambda \|\boldsymbol{s}\|_1 \} \quad (10)$$

where $\lambda > 0$ is a regularisation parameter that weights the importance of sparsity. In this paper the ℓ_1-norm regularization is solved using the Sparse Reconstruction by Separable Approximation (SpaRSA) algorithm [22] (see Table 1). After estimating the amplitude vector $\hat{\boldsymbol{s}}$, the location of the artefacts can be obtained directly by searching for the non-zero components $s_{\boldsymbol{q}}$ at the corresponding axial coordinates $\underline{z}_q$.

For comparative analysis, this study also evaluates algorithms that do not incorporate prior sparse information, such as the Least Squares (LS) method. The LS method is functionally equivalent to the Maximum Likelihood (ML) method, assuming that the residual errors between the measured sound pressure and the predictive model follow a normal distribution [23]. Notably, the ML approach has been employed for the detection of blockages or leakages in pipes, as demonstrated in prior studies [6] [12]. In the context of this paper, the inverse problem described in Equation Eq. (6) is addressed using the LSQR algorithm, implementing the LS/ML method [24]. The proposed technique for the localization of artefacts in the pipe with mobile compensation using ℓ_1-norm regularization SR is summarized in Table 1.

Table 1. Algorithm 1 - frequency domain SR estimation with ℓ_1-norm regularization with SpaRSA [22] to localize artefacts in a pipe.

Task: To estimate the location of artefacts in the pipe $\hat{\boldsymbol{s}}$
Input: Excitation chirp signal $A_{00}(t)$, response signal from six microphones $\boldsymbol{p}_m(t)$ m=1:6

Plane wave reconstruction: $\boldsymbol{p}(t) = \sum_{m=1}^{6} \boldsymbol{p}_m(t)$
Fast Fourier transform: $\boldsymbol{p}(\omega) = \mathcal{FFT}\{\boldsymbol{p}(t)\}$, $\boldsymbol{A_{00}}(\omega) = \mathcal{FFT}\{\boldsymbol{A_{00}}(t)\}$
Transfer matrix: $\boldsymbol{h}(\omega, \boldsymbol{z}_q) = \boldsymbol{A_{00}}(\omega) e^{-2\mathrm{i}\lvert k_0(\omega)\boldsymbol{z}_q\rvert - 2\mathrm{sgn}(\boldsymbol{z}_q)[\mathrm{i}k_0(\omega)v_r t_r(\omega)]}$
Initialization: k=1, $\mathbf{A} = \boldsymbol{h}$, $\boldsymbol{x}_1 = \boldsymbol{p}$, $\tau_1\mathbf{I} = \mathbf{A}^T\mathbf{A}$, tolerance $\varepsilon = 10^{-5}$ [22], parameter $\lambda = 0.001$ [22]
Iteration: 1. $\lambda_k = \max\{0.1\lVert\mathbf{A}^T\boldsymbol{x}_k\rVert_\infty, \lambda\}$ [22].
2. Exploit soft shrinkage [22]: $\boldsymbol{s}_{k+1} = \mathrm{shrink}(\boldsymbol{s}_k - \mathbf{A}^T(\mathbf{A}\boldsymbol{s}_k - \boldsymbol{x})/\tau_k, \lambda_k/\tau_k)$ (where $\mathrm{shrink}(x, y) = \mathrm{sgn}(x)\max\{\lvert x\rvert - y, 0\}$)
3. Update the step size [22]: $\tau_k = \frac{(\boldsymbol{s}_{k+1}-\boldsymbol{s}_k)^T(\boldsymbol{\nabla\vartheta}(\boldsymbol{s}_{k+1})-\boldsymbol{\nabla\vartheta}(\boldsymbol{s}_k))}{(\boldsymbol{s}_{k+1}-\boldsymbol{s}_k)^T(\boldsymbol{s}_{k+1}-\boldsymbol{s}_k)}$
4. If $\frac{\lVert\boldsymbol{s}_{k+1}-\boldsymbol{s}_k\rVert}{\boldsymbol{s}_k} \leq \varepsilon$, go to step 5**.** Otherwise, return to step 2 [22]
5. $\boldsymbol{s}_{k+1} = \boldsymbol{x} - \mathbf{A}\boldsymbol{s}_{k+1}$
6. If $\lambda_k \leq \lambda$, stop**;** Otherwise k=k+1, and return to step 1.
Output: $\hat{\boldsymbol{s}} = \boldsymbol{s}_k$

1

2 For comparison, two more algorithms are presented in Tables 2 and 3. Table 2 presents the
3 algorithms based on straightforward deconvolution without mobile compensation. Table 3
4 presents the LS method with compensation for a moving inspection robot with a 6-microphone
5 array. The deconvolution method is used here for comparison with other algorithms since the
6 location of the artefacts can also be estimated directly using the peaks of the envelope of the
7 impulse responses.

8 Table 2. Algorithm 2 - straightforward deconvolution without mobile compensation.

Task: To estimate the location of artefacts in the pipe $\hat{\boldsymbol{s}}$

Input: Excitation chirp signal $A_{00}(t)$, response signal from six microphone $\boldsymbol{p}_m(t)$ m=1:6
Plane wave reconstruction: $\boldsymbol{p}(t) = \sum_{m=1}^{6} \boldsymbol{p}_m(t)$
Fast Fourier transform: $\boldsymbol{p}(\omega) = \mathcal{FFT}\{\boldsymbol{p}(t)\}$, $\boldsymbol{A_{00}}(\omega) = \mathcal{FFT}\{\boldsymbol{A}_{00}(t)\}$
Transfer function: $\boldsymbol{h}(\omega) = \boldsymbol{p}(\omega)/\boldsymbol{A_{00}}(\omega)$
Inverse Fourier transform: $\hat{\boldsymbol{s}} = i\mathcal{FFT}\{\boldsymbol{h}(\omega)\}$
Output: $\hat{\boldsymbol{s}}$

Table 3. Algorithm 3 - frequency domain LS with mobile compensation.

Task: To estimate the location of artefacts in the pipe $\hat{\boldsymbol{s}}$
Input: Excitation chirp signal $\boldsymbol{A}_{00}(t)$, Response signal from six microphone $\boldsymbol{p}_m(t)$ m=1:6
Plane wave reconstruction: $\boldsymbol{p}(t) = \sum_{m=1}^{6} \boldsymbol{p}_m(t)$
Fast Fourier transform: $\boldsymbol{p}(\omega) = \mathcal{FFT}\{\boldsymbol{p}(t)\}$, $\boldsymbol{A_{00}}(\omega) = \mathcal{FFT}\{\boldsymbol{A}_{00}(t)\}$
Transfer matrix: $\boldsymbol{h}(\omega, \boldsymbol{z}_q) = \boldsymbol{A_{00}}(\omega) e^{-2\mathrm{i}\lvert k_0(\omega) z_q \rvert - 2\mathrm{sgn}(z_q)[\mathrm{i} k_0(\omega) v_r t_r(\omega)]}$
LS solution: $\hat{\boldsymbol{s}} = (\boldsymbol{h}^{\mathrm{H}}\boldsymbol{h})^{-1}\boldsymbol{h}^{H}\boldsymbol{p}$
Output: $\hat{\boldsymbol{s}}$

3. Experimental setup

The acoustic sensing system was mounted on a remotely controlled robot (iRobot Looj 330 by iRobot, www.irobot.com) which can move along a pipe invert with a constant velocity of 0.1 m/s. The acoustic equipment used in this work consisted of a loudspeaker and a six-microphone array. The array, speaker, processor (Raspberry Pi 4), power amplifier for the speaker, ADC, and DAC used for data acquisition are shown in Figure 4(d). The sampling rate was f_s =16 kHz. A 100 – 5000 Hz sweep sine with duration 20 s was used as a basic excitation signal. The duration of the acoustic response of the pipe used to calculate the fast Fourier transform in Eq. (6) was T = 21 s. This corresponded to a signal realization with L = 80000 samples (from 200

to 4000 Hz with frequency resolution 0.0475 Hz). The speaker and the centre of the microphone array were located at the centre of the pipe with a 5 mm positional mean error initially, although this could change due to the robot movement inside the pipe. The microphone type used in this experiment was MSM321A3729H9CP by MEMSensing Microsystems Co. Ltd. The Visaton 2242 speaker with the 32mm diameter was driven with a 3W power supply.

The diameter of the air-filled pipe section shown in Figure 4(a) was 150mm. The straight section had a 100 mm diameter lateral connection attached at 90^{o} (see Figure 4(b)). The detailed lengths of the pipe sections in each experiment are described in the following text. A sandbag was placed in the pipe closely to the lateral connection as shown at the left of Figure 4(c) to validate the performance of the proposed algorithm for separating overlapped acoustic echoes. The concrete blockage at the right of Figure 4(c) was also validated in the experiments, but without the results shown in this paper since it exhibits similar results as the sandbag. The straight section was terminated with a heavy wooden board at each to illustrate the idea of full reflections from the terminated ends and to help validate the proposed algorithm.

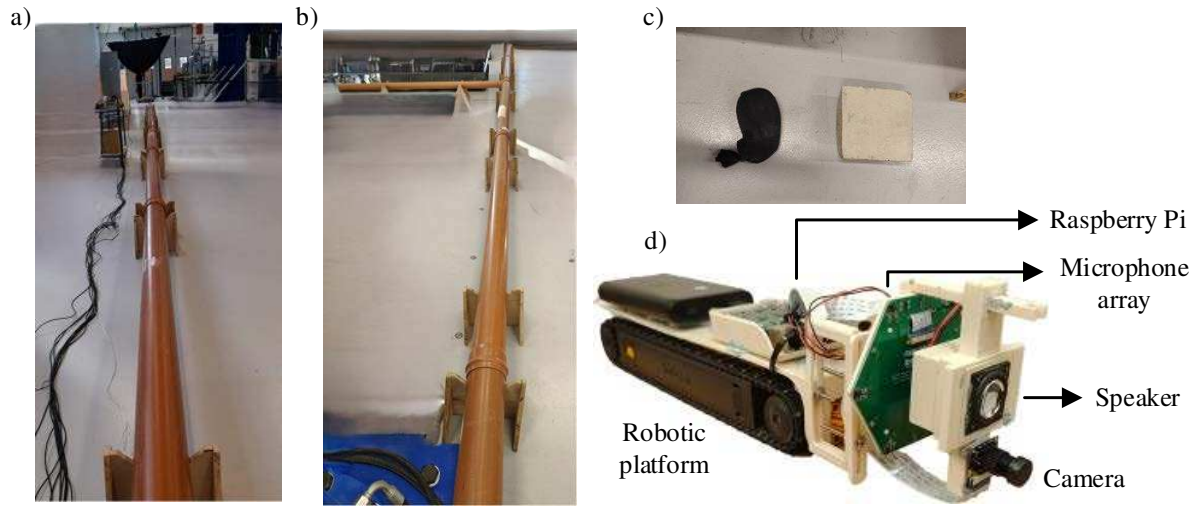

Figure 4. (a) the straight 150mm pipe, (b) the straight pipe with a single 100mm diameter lateral connection, (c) blockage samples, (left) a sandbag, (right) a 150mm width, 150mm length semi-

circular (150 mm diameter) concrete in-pipe blockage included to illustrate the size of the sandbag, (d) the robotic platform with the speaker and array of acoustic sensors

4. Results

This section presents results obtained with the proposed deconvolution, LS and SR algorithms to localize in-pipe artefacts/defects. The location of the artefacts/defects can be estimated by the coordinates associated with the peaks, which can be determined from a find peak function (e.g. *@findpeaks* in Matlab). These results were obtained using a static and moving inspection robot in a re-configurable straight pipe with/without a blockage and lateral connection.

4.1 Testing with a static robot

4.1.1 Straight pipe

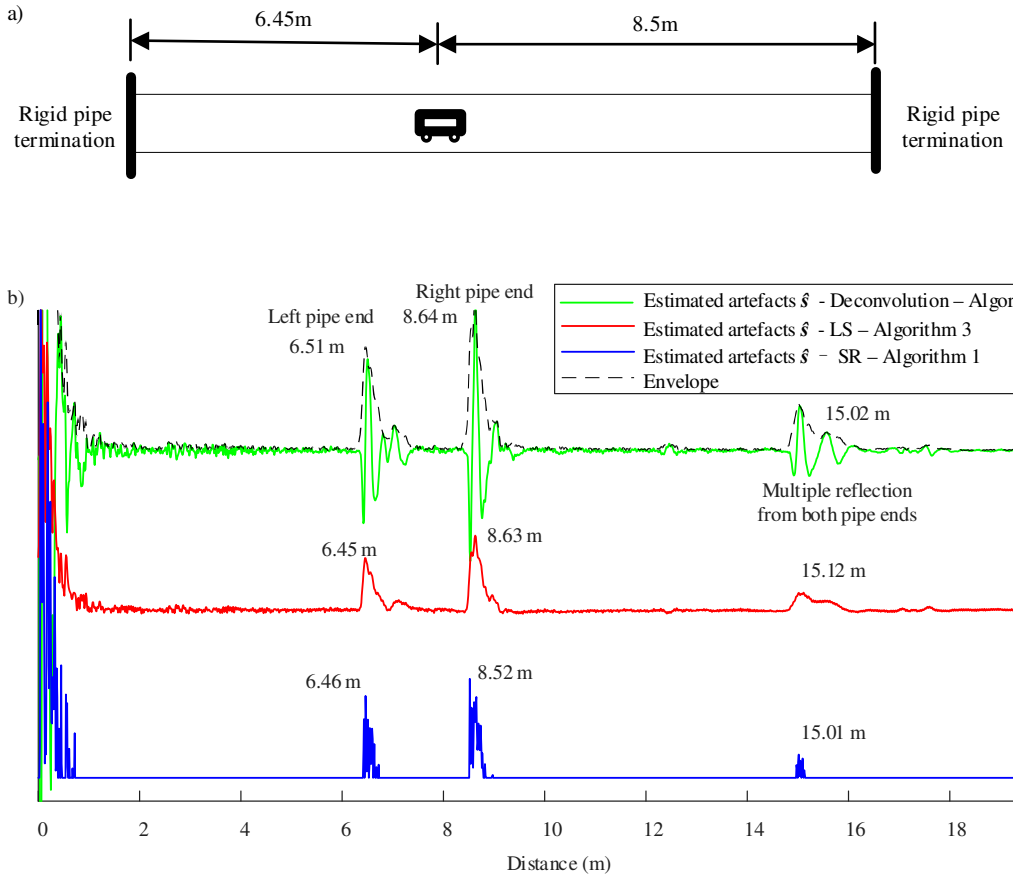

Figure 5. (a) an illustration of a robot in the straight pipe with two rigid terminations; (b) artefact/defect estimation using deconvolution, LS and SR algorithms in the frequency range of 200-4000 Hz.

As shown in Figure 5 the deconvolution result of the impulse response is presented with the temporal coordinates normalized by the half of the sound velocity to illustrate the spatial location of the artefacts/defects, which will be extensively used in this paper. The normalization of either the impulse response or the predicted reflection amplitude (denoted as $\hat{\boldsymbol{s}}$ in Algorithms 1-3) was applied for the localization. Consequently, this normalization results are not necessarily represented on the y-axis within the context of this paper. Compared with the deconvolution and LS results, the SR using ℓ_1-norm regularization presents a curve for artefacts' echoes that has a better definition in the spatial distribution, and less noise due to the introduction of sparsity than with the other two methods. The estimated location of the pipe terminations using SR with ℓ_1-norm regularization achieved a less than 0.4% error in terms of the overall sensing distance. This compares favourably against a 1% error in location estimation using deconvolution and LS. Note that the distance was estimated at the peak of the envelope for deconvolution, whereas the LS and SR can be estimated directly at the peak values. The sensing error ε was calculated as:

$$\varepsilon = |z_M - z_R|/z_R \tag{11}$$

where z_M and z_R are the measured and real distance of the pipe features respectively. Although both the reflections from the pipe end were caused by pipe terminations made from the same wooden board, the amplitude of the front echoes are slightly stronger than the echoes coming from the back of the robot. This is because the robot itself presents an object that creates acoustic reflections that can scatter sound and so affect the acoustic signal received by the

microphone array. The secondary reflection from both pipe ends was located around 15 m in the estimated artefacts curves and corresponded to the length of the whole pipe.

4.1.2 Pipe with lateral connection

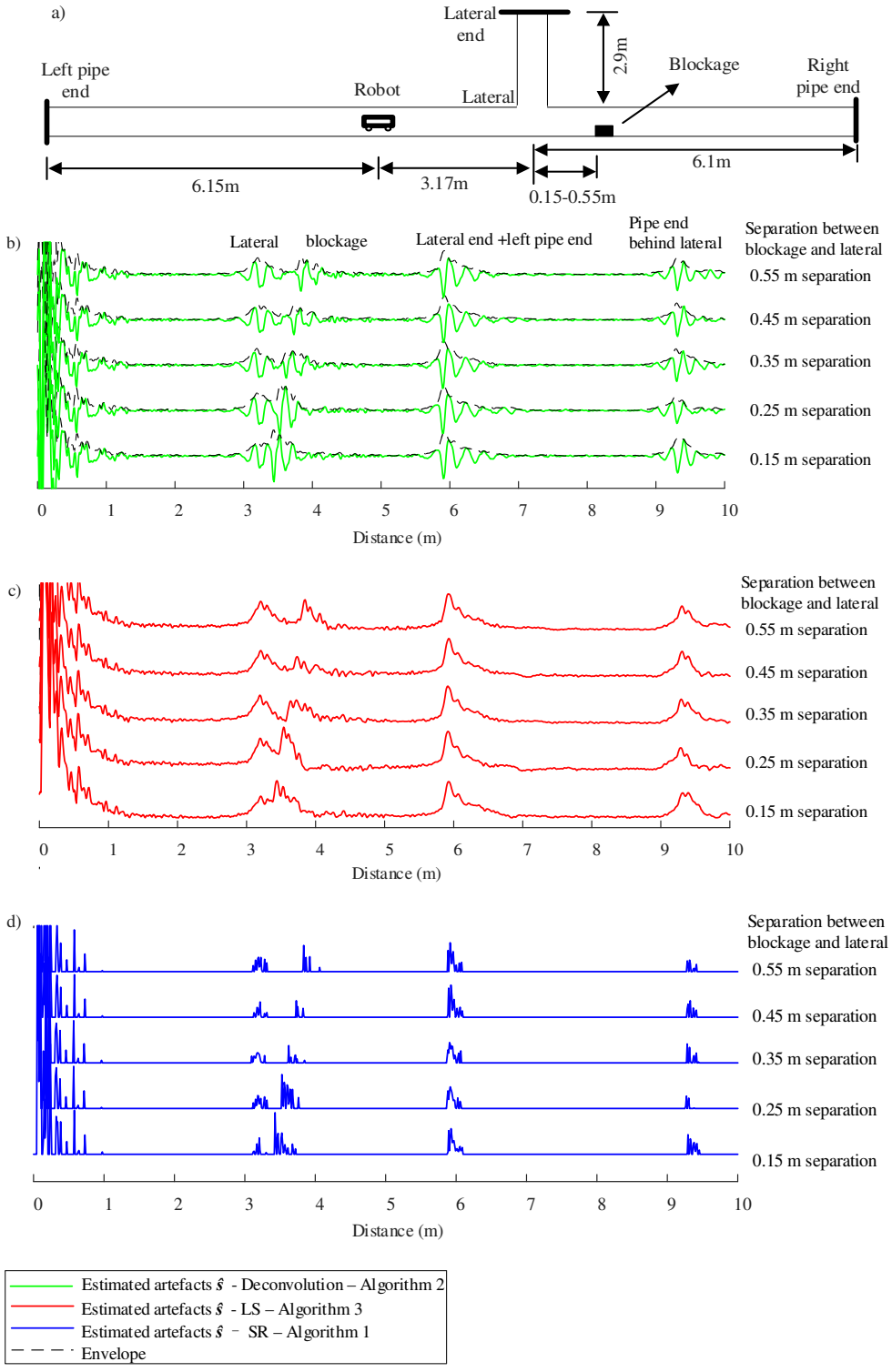

Figure 6. (a) an illustration of a static robot in a pipe with a closely spaced lateral connection and blockage (sandbag); (b)-(d) artefact/defect location estimation using deconvolution, LS and SR with ℓ_1-norm regularization, respectively. The frequency range used in LS and SR algorithms was limited to 200-4000 Hz.

Figure 6 compares the artefact location estimation with the microphone array using deconvolution, LS and SR with ℓ_1-norm regularization when there is a blockage closely placed behind the lateral connection. The distance between the robot and the left pipe end was almost the same as the robot to the lateral end, thereby resulting in the overlapping of reflections. The separation spacing of the lateral and blockage was calculated from the centre of the lateral to the closest edge of the blockage (where a sandbag in Figure 4(b) is used). As shown in Figure 6, the estimation of the location of the two artefacts using deconvolution and LS was problematic because the echoes from lateral connection and blockage largely overlapped when their separation was within the 0.15-0.55 m range. In particular, when the separation became comparable to the acoustic wavelength at the higher end of the frequency spectrum ($\lambda =$ 85 mm at 4 kHz) the deconvolution did not allow for the separation of the two echoes as shown in Figure 6(b). This can cause problem for blockage localisation near a lateral connection or close to a manhole [8]. In comparison, the SR estimation using ℓ_1 norm regularization robustly separated these two echoes even when their spacing was only 0.15 m. This result provides the advantage of proposed algorithm for the application of artefact/defect localisation in a pipe.

It is also worth noting that the lateral connection and blockage have rather different reflection coefficients that are frequency dependent [5]. As discussed in Ref. [8], the maximum reflection coefficient of the plane wave mode from lateral connection is close to the low-frequency start of the excitation chirp (100 Hz in this study) and gradually reduces to nearly zero at the first cut-on frequency of the pipe (1340 Hz for 150 mm pipe). Above the first cut-on frequency, this reflection coefficient stays relatively small compared to that for a blockage. Therefore, the

selected frequency range can significantly affect the performance of the proposed frequency domain SR estimation algorithm. The low frequency components contain more reflected sound from the laterals but provides a lower resolution to separate and localize closely spaced artefacts. The higher frequency sound waves can offer much higher precision, but these are not always reflected well from a lateral connection particularly when it is behind the robot. This aspect deserves closer investigation and can be optimized through a combination of the theoretical model proposed in Ref. [5] and the SR algorithm proposed in this paper.

Figure 7 shows the artefact/defect localization estimation for a small blockage behind a lateral connection with a 0.35 m separation. In this experiment the 200-1000 Hz signals with the minimum wavelength of $\lambda = 340$ mm and below the first cut-on frequency of 1340 Hz were used. This frequency range did not allow for the discrimination between the blockage and lateral connection with either the SR algorithm or the other two methods due to a relatively low resolution attained with this frequency range. In particular, the SR algorithm results in several peaks all corresponding to the same artefact. These peaks were difficult or impossible to separate. Such an example illustrates the importance of using the microphone array to increase as much as possible the maximum frequency in the plane wave in Eq. (8) beyond the first cut-on frequency of non-axisymmetric modes to localize accurately and separate the artefacts.

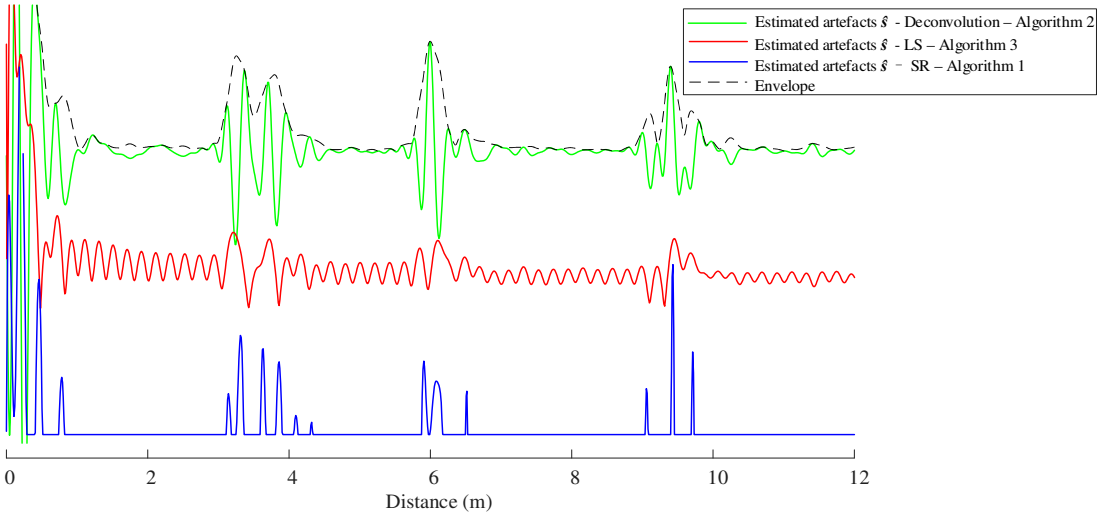

Figure 7. The effect of a reduced frequency range on the resolution of the three artefact localisation algorithms: deconvolution (green solid line), LS (red solid line) and SR with ℓ_1-norm regularization (blue solid line), respectively. The frequency range is 200-1000 Hz.

4.2 Testing with moving robot

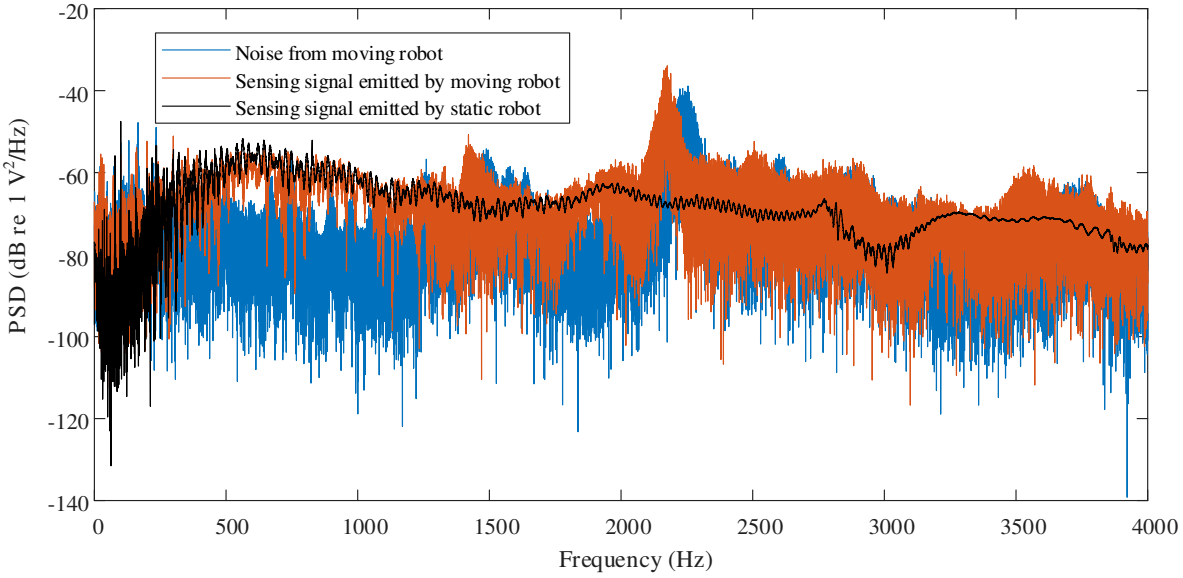

Figure 8. The narrow band power spectrum density of noise from the moving robot and 20 s chirp excitation signal emitted by the robot.

A robot moving in a pipe makes significant stationary noise as shown in Figure 8. This figure presents the power spectrum of noise emitted by the robot's locomotion system and spectra of the sensing signals emitted by the static and moving robot. The SNR over 100-4000 Hz without the deconvolution was estimated at around 0 dB for a single microphone based on the spectral average (see Figure 8). The robot's locomotion noise was generally broad band but has peaks around 2.2 kHz.

4.2.1 Localization results for a straight pipe

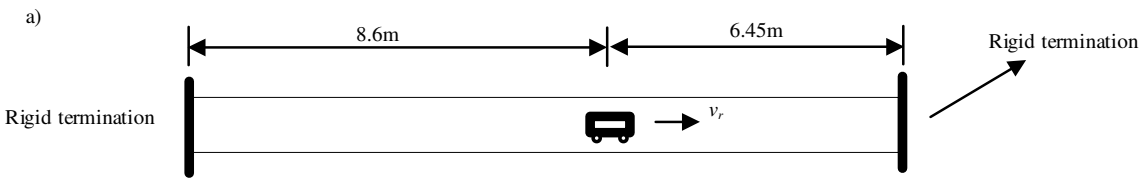

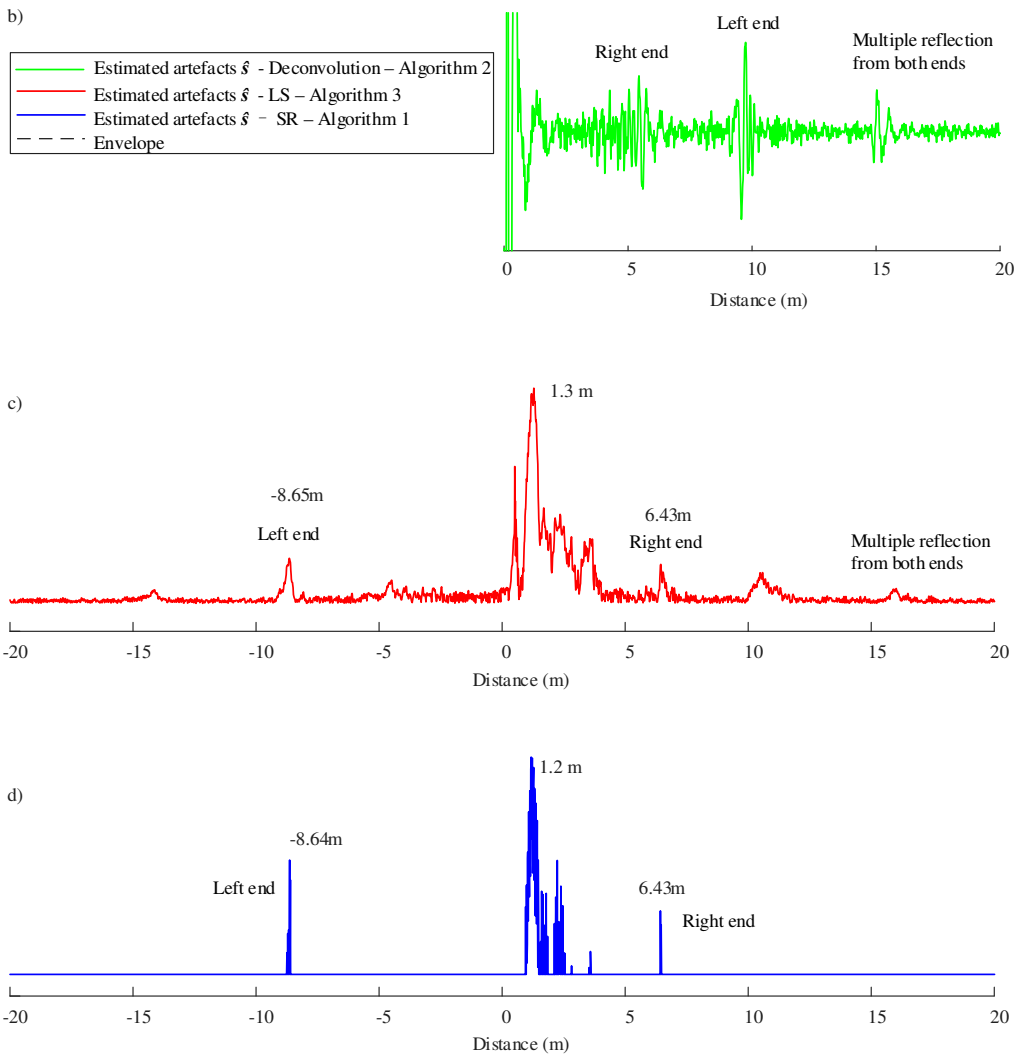

Figure 9. (a) an illustration of a moving robot in a straight pipe with rigid terminations at the both ends; (b) the estimated location of the pipe terminations using deconvolution without mobile compensation (green solid line); (c) LS with mobile compensation (red solid line), and (d) SR with ℓ_1-norm regularization with mobile compensation (blue solid line). The frequency range is 200-4000 Hz.

Figure 9 shows the estimated location of the pipe ends using deconvolution, LS and SR algorithms. Without mobile compensation, the acoustic impulse response obtained through deconvolution was noisy particularly near the right pipe end making the identification and localization of these artefacts difficult. The LS and SR algorithms with mobile compensation show the location of the pipe ends much more clearly. Since the LS algorithm does not use the

prior knowledge of the sparsity nature of pipe artefacts, it tends to have more noisy disturbances of the estimated artefacts vector $\hat{\boldsymbol{s}}$ than the SR. The proposed SR algorithm using ℓ_1-norm regularization showed a significantly more robust estimation of both the direction and location of the pipe artefacts with a less than 0.5% error in terms of sensing distance.

Although the mobile compensation can improve the estimation accuracy and tends to be robust against noise, the acoustic source can cover a relatively long distance while taking measurements creating a localization "blind zone" whose length is dependent on the moving velocity and chirp duration. In the reported experiments the robot's velocity was 0.1 m/s suggesting that the robot would cover a distance of around 2 m for a 20 s chirp excitation. With the twice velocity compensation term in Eq. (4), the reconstructed excitation covers twice of the robot's moving distance which is 4 m. Therefore, LS presents a 4 m excitation pulse at the spatial range 0.2-4 m, whereas SR method shows a slightly shorter excitation pulse ranging 1-3.7 m. This "blind zone" may cause some difficulties for the detection of defects within its range. The peaks of the source pulse from LS and SR are around 1.3 m and 1.2 m, respectively (as shown in Figure 9(c) and Figure 9(d)), which present a slight offset from the initial robot location (zero coordinate). One of the solutions to reduce the effects from "blind zone" is moving the robot further away from the artefacts (e.g. reversing the robot) so that the disturbance of the "blind zone" pulse can be positioned in the other direction of the artefacts. This will be discussed in the next section in detail.

It is worth noting that the multiple reflections that travelled twice the pipe length and received by the microphone array on the moving robot were not significantly affected by the robot velocity, assuming that the robot velocity was much smaller than the sound velocity $v_r \ll c_0$. Therefore, the deconvolution did not require to compensate for the Doppler shift. Figure 9(b) shows that the multiple reflections measured through the deconvolution without using the mobile compensation can be used to estimate the pipe length, which was 15 m in the reported

experiments. However, in Figure 9(c) this feature was smeared in the 14-16 m range with both positive and negative coordinates after the mobile compensation using the LS algorithm. In Figure 9(d) the multiple reflections were cancelled due to their significantly small amplitude. Hence, the pipe length will not be identified directly using the feature of multiple reflection as discussed in Ref. [8, 14], but by the summation of the distance from left and right reflections.

4.2.2 Localization results for a pipe with a lateral connection

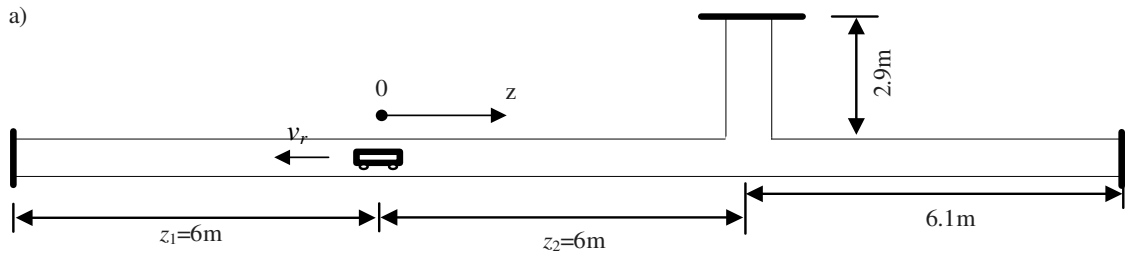

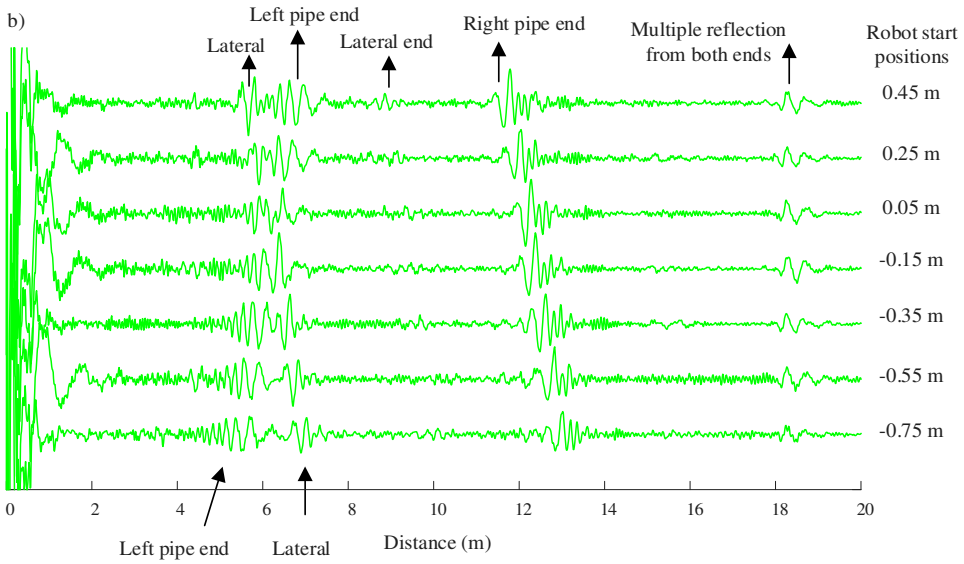

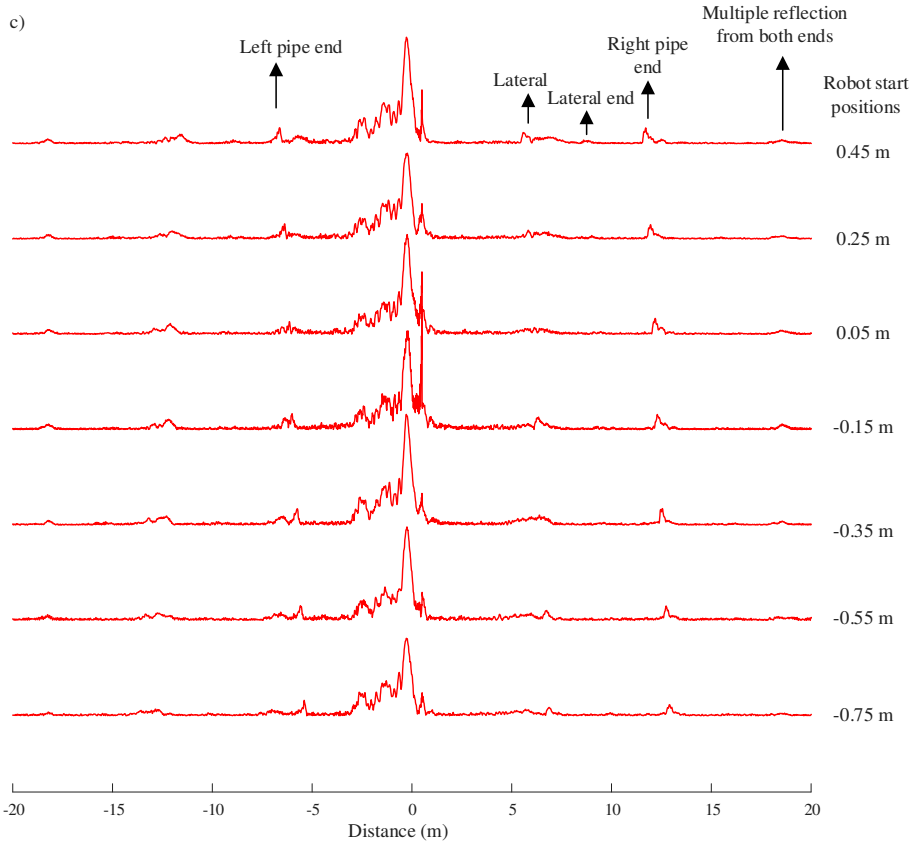
c)
Left pipe end
Lateral
Lateral end
Right pipe end
Multiple reflection from both ends
Robot start positions
0.45 m
0.25 m
0.05 m
-0.15 m
-0.35 m
-0.55 m
-0.75 m
-20
-15
-10
-5
0
5
10
15
20
Distance (m)

1

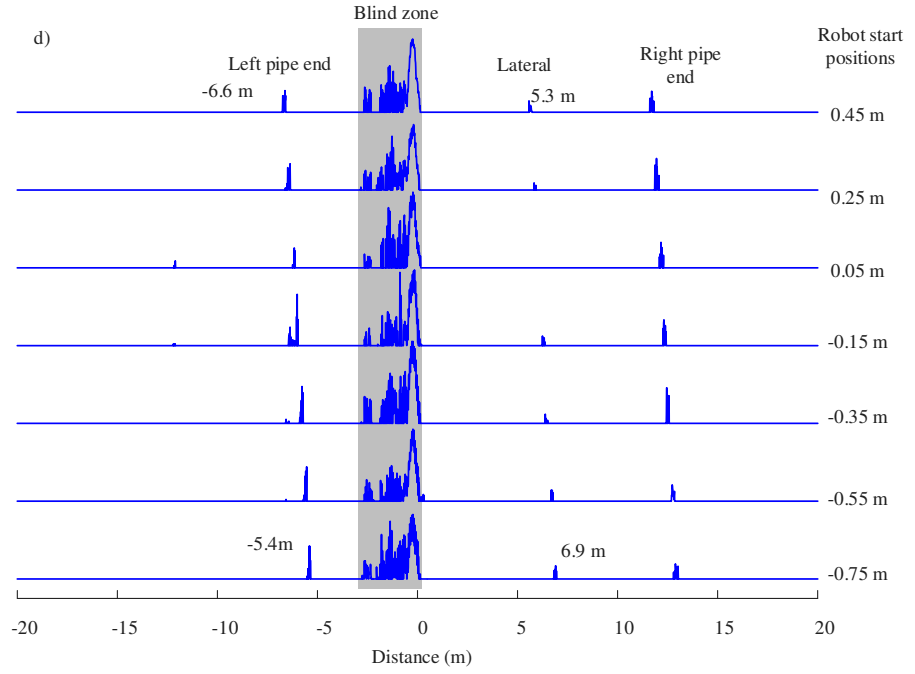
d)
Blind zone
Left pipe end
-6.6 m
Lateral
5.3 m
Right pipe end
Robot start positions
0.45 m
0.25 m
0.05 m
-0.15 m
-0.35 m
-0.55 m
-0.75 m
-5.4m
6.9 m
-20
-15
-10
-5
0
5
10
15
20
Distance (m)

2

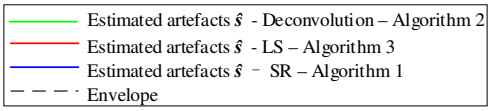
Estimated artefacts ŝ - Deconvolution – Algorithm 2
Estimated artefacts ŝ - LS – Algorithm 3
Estimated artefacts ŝ – SR – Algorithm 1
Envelope

3

Figure 10. (a) an illustration of a moving robot in a rigidly terminated pipe with a lateral connection; (b) the estimated location of the lateral connection and pipe ends using deconvolution without mobile compensation; (c) LS with mobile compensation; and (d) SR with ℓ_1-norm regularization with mobile compensation. The frequency range is 200-4000 Hz.

When the robot was located in the middle between two pipe artefacts, i.e. an equal distance to the pipe end on the left and the lateral connection on the right as shown in Figure 10(a), the acoustic echoes from these two artefacts overlapped making it difficult to separate them. In this experiment, the robot starting position was moved progressively from the centre of this pipe section as shown in Figure 10(a) to examine the performance of the three localization algorithms when dealing with overlapped echoes coming from these two artefacts. As shown in Figure 10(b), the acoustic echoes from the left pipe end and the lateral connection on the right overlap in the acoustic impulse response obtained through the deconvolution. The LS and SR algorithms can improve the localization estimation of these artefacts and determine the direction of their echoes. As shown in Figure 10(c), the left pipe end and lateral connection on the right present closely clustered peaks in the estimated acoustic response unless the robot has moved farther than ±150mm from the initial middle location. The location and direction of these pipe artefacts can be accurately estimated using the SR algorithm when the overlap separation is larger than 0.3 m as shown in Figure 10(d).

The acoustic source on the moving robot covered around 2.5 m during the data acquisition causing the presence of a blind zone for the proposed localisation algorithms. Note that the blind zone in Figure 10(d) was in the negative coordinates since the robot was reversing from the lateral with negative velocity ($v_r = -0.1$m/s), whereas in Figure 9, the blind zone was in the positive coordinates because the robot was moved in the positive direction (at $v_r = +0.1$m/s). In this way, the blind zone can be removed by taking consecutive measurements while moving the robot backwards and then fusing the collected data.

4.2.3 *Chirp duration effects*

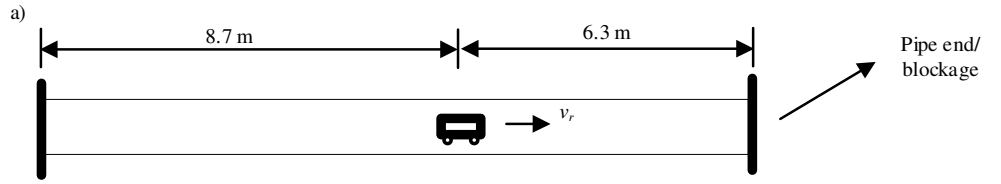

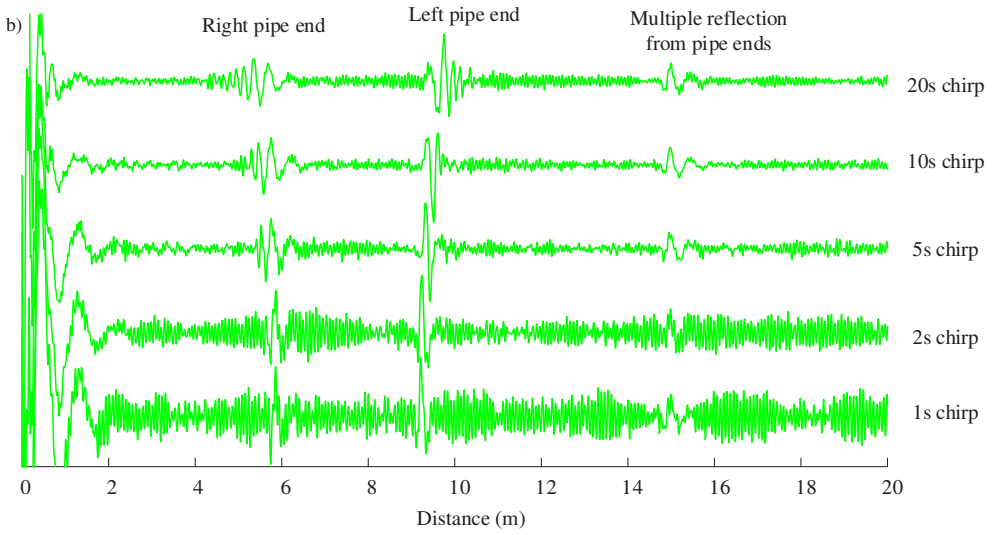

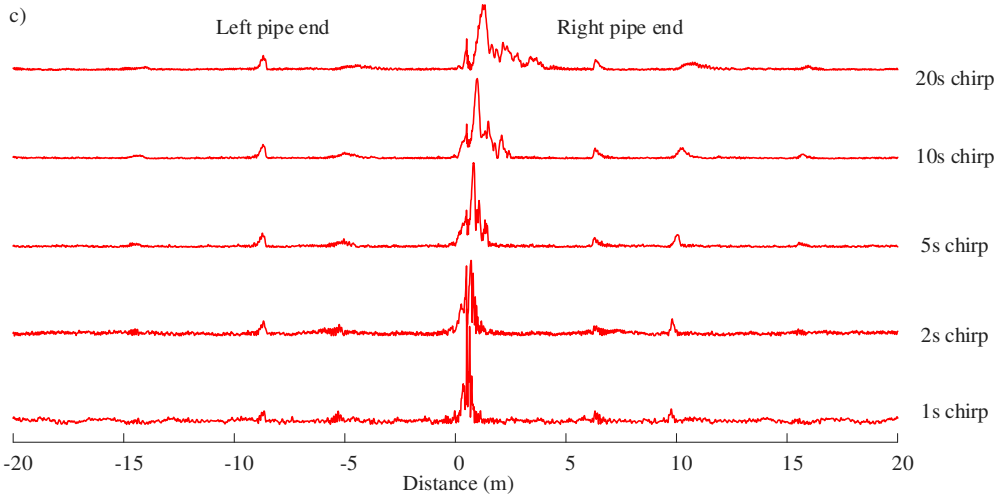

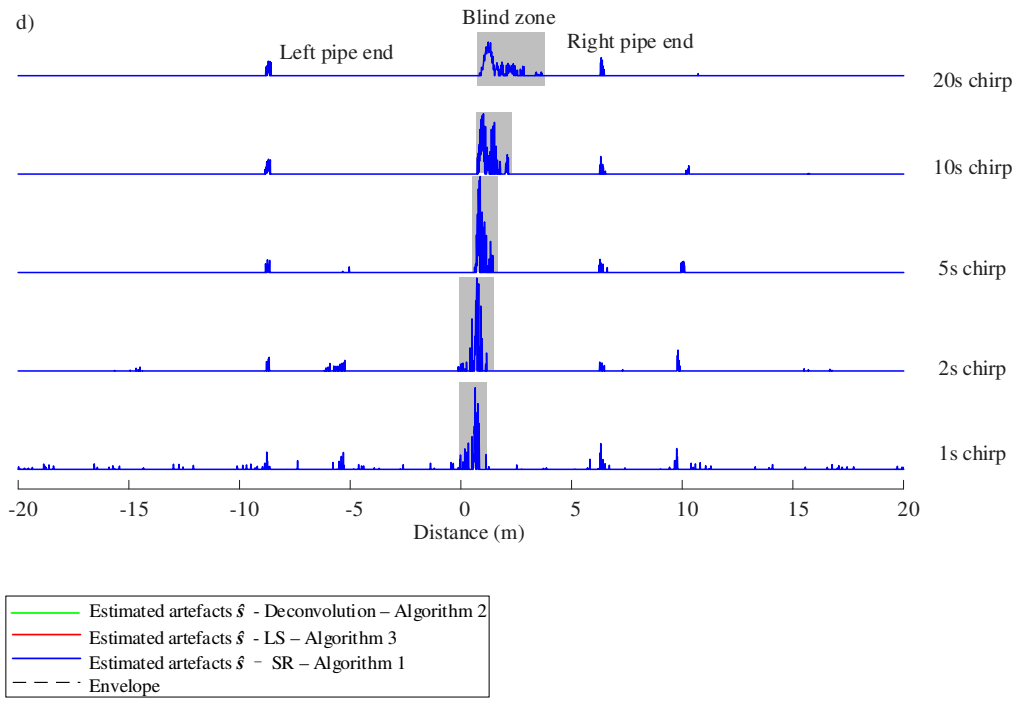

Figure 11. (a) an illustration of the moving robot in a straight pipe with terminated ends. The effect of the chirp duration on the quality of: (b) deconvolution method without mobile compensation; (c) LS algorithm with mobile compensation; and (d) SR algorithm with ℓ_1-norm regularization with mobile compensation, respectively. The frequency range is 200-4000 Hz. Blind zone is shown in grey.

As shown in Figure 11(b), the signal to noise ratio tends to increase with the chirp duration resulting in a better-quality acoustic response predicted through deconvolution. The SNR of the mean value from the 6 microphones after deconvolution with a single measurement were 10.5dB, 7.1dB, 2.2dB, -0.2dB and -3.3dB for 20s, 10s, 5s, 2s, and 1s chirps over the frequency range 200-4000 Hz, respectively. For very short duration sensing, the location of the robot and artefacts can be estimated without mobile compensation using deconvolution when the robot's velocity is relatively small (e.g. tenths of cm/s). For example, the 5 s chirp can provide a reasonable location (within 5% error in terms of sensing distance) of the artefacts with relatively sufficient signal to noise ratio while the robot is moving at 0.1 m/s (SNR is around 2 dB). However, the noise (e.g. less than 0 dB for 2 s chirp) generated by robot can lead to

localization inaccuracies particularly for small blockages (e.g. <20% blockage area ratio), which is attributed to the possibility of the reflective pulse becoming submerged within the noise. Whereas for longer duration of sensing, the estimation of the location of the robot and artefacts requires the mobile compensation, although the signal to noise ratio is relatively large (e.g. >10 dB for 20s chirp). The SR algorithm proposed using ℓ_1-norm regularization presents a more robust estimation towards noise of the directional location of both pipe ends with 20 s chirp duration, compared with the other two algorithms.

Reducing the chirp duration can result in a shorter distance required for the robot to move while taking measurements. A shorter distance can be insufficient for the adopted LS and SR algorithms to discriminate the direction of the acoustic echo from artefacts. For example, there is a mis-predicted feature at around 10 m of the right side for a chirp sensing at 10 s as shown in Figure 11(d). Note that the right blockage in the case of 10 s chirp is located at around 10.5 m the location estimate has a is 0.5 m error. This mis-estimation of the direction is due to the robot moving an insufficient distance during the measurement. The mis-estimation of the location is due to the amplitude of the speaker response being maximized in the range 1-2 kHz, which is associated to the maximized acoustic echo amplitude from the artefacts when the robot was emitting a chirp at 1-2k Hz. This phenomenon is also presented with the slight shift of the robot initial location, as shown in Figure 11b.

5. Conclusions

This paper proposed a Sparse Representation method for the localization of artefacts/defects in an air-filled pipe using a circular microphone array on a static and moving inspection robot. Compared with a static robot, the moving robot enables the determination of the direction of acoustic echoes reflected from the artefacts and defects located in front of and behind the moving robot.

The use of a microphone array enables the extraction of the plane wave mode in the frequency range above the first cut-on frequency of the pipe, which is crucial for the precise localization and separation of closely situated artifacts and defects. The proposed algorithm based on SR estimation with ℓ_1-norm regularization makes use of the sparse nature of pipe artefacts and defects which compensates for the phase shift induced by a moving robot and suppresses the noise of the moving robot to provide a robust estimation of the location of artefacts/defects. In contrast to LS, the SR method demonstrates superior robustness and accuracy in estimating the location of pipe artifacts/defects for both static and mobile robotic systems. It also enables a moving robot to detect the direction to the artefact and separate overlapped acoustic echoes from two or more closely located artefacts and defects.

This proposed algorithm is expected to work in pipes filled with other fluids other than air e.g. water/natural gas. Given the distinct sound velocity inherent in such mediums, the analysed frequency range necessitates adjustment to accommodate the wavelength corresponding to the sensitive dimensions of defects/artefacts. The paper assumes that the pipes are air-filled, however many drainage pipes are over-sized for typical stormwater flows, so may only be filled with water to a depth that would be 10-15% of the pipe diameter. There may be some occasions when the level of water changes gradually with the distance. This paper does not consider these situations because they are relatively rare as water generally trends to a uniform flow depth to balance frictional losses with energy provided by gravitation. Furthermore, the pipes (e.g., plastic pipes) may undergo ovalization or exhibit other alterations in shape due to practical circumstances. However, the method we propose (Eq. (4)) is based on the extraction of the plane wave and it is perfectly valid to use in oval pipes with exactly the same microphone array and speaker placed in the middle of the pipe cross-section to minimize the impact of shape conditions on the measurements.

The proposed algorithm is able to separate and detect the overlapped echoes with a less than 0.4% error in terms of the sensing distance provided that the overlap is greater than 0.15m for a static robot and greater than 0.35m for moving robot. This error is quoted for the robot's speed of 0.1 m/s. This error would reduce as the robot speed would increase. This paper also discusses the effects from excitation duration which is associated with the signal to noise ratio (SNR) on the estimation accuracy. It is shown that the method works for SNRs down to around 2dB and chirp durations of around 5 seconds. For higher robot velocities which are still significantly smaller than the sound speed, e.g. 1m/s, this approach should still work with a shorter chirp and lower noise level to minimise the blind zone. At lower speeds, this method typically employs an extended chirp duration over the distance covered, enabling effective phase compensation to distinguish sound from opposing directions. This work paves the way for the development of acoustic methods able inspect fluid filled pipes, for artefacts and defects with autonomous mobile inspection robots.

Conflict of Interest statement and Data Availability

All authors declare that they have no conflict of interest or financial conflicts to disclose. The data that support the findings of this study are available from the corresponding author upon reasonable request.

Acknowledgement

This work is supported by the UK Engineering and Physical Sciences Research Council (EPSRC) Programme Grant No. EP/S016813/1. The authors would like to gratefully thank Dr. Will Shepherd and Mr. Paul Osbourne for kindly helping with the design of the blockages and providing other experimental facilities.

1 **References**

2

[1] “Discover water: treating sewage,” [Online]. Available: https://discoverwater.co.uk/treating-sewage. [Accessed 01 02 2023].

[2] W. UK, “New proof that flushing wipes is a major cause of sewer blockages,” 12 12 2017. [Online]. Available: https://www.water.org.uk/news-views-publications/news/new-proof-flushing-wipes-major-cause-sewer-blockages. [Accessed 20 11 2023].

[3] E. A. Shrimpton, D. V. Hunt and C. D. Rogers, “Justice in (English) water infrastructure: a systematic review.,” *Sustainability ,* vol. 13, no. 6, p. 3363, 2021.

[4] T. L. Nguyen, A. Blight, A. Pickering, G. Jackson-Mills, A. R. Barber, J. H. Boyle, R. Richardson, M. Dogar and N. Cohen, “Autonomous control for miniaturized mobile robots in unknown pipe networks,” *Frontiers in Robotics and AI,* vol. 9, no. 16, 2022.

[5] Y. Yu, A. Safari, X. Niu, B. Drinkwater and K. V. Horoshenkov, “Acoustic and ultrasonic techniques for defect detection and condition monitoring in water and sewerage pipes: A review,” *Applied Acoustics,* vol. 183, no. 0003-682X, p. 108282, 2021.

[6] S. Nasraoui, M. Louati and M. S. Ghidaoui, “High resolution acoustic identification of clusters of small blockages in fluid-filled pipe using maximum likelihood estimation,” *The Journal of the Acoustical Society of America,* vol. 153, no. 5, p. 3086, 2023.

[7] J. M. Aitken, M. H. Evans, R. Worley, S. Edwards, R. Zhang, T. Dodd, L. Mihaylova and S. R. Anderson, “Simultaneous localization and mapping for inspection robots in water and sewer pipe networks: A review,” *IEEE Access ,* vol. 9, 2021.

[8] Y. Yu, R. Worley, S. Anderson and K. V. Horoshenkov, “Microphone array analysis for simultaneous condition detection, localization, and classification in a pipe,” *The Journal of the Acoustical Society of America,* vol. 153, no. 367 , p. 367–383, 2023.

[9] Y. Yu, K. V. Horoshenkov and S. Tait, “Microphone array analysis of the first non-axisymmetric mode for the detection of pipe conditions,” *The Journal of the Acoustical Society of America,* vol. 155, no. 1, pp. 575-587, 2024.

[10] D. Zhong, D. Yang and M. Zhu., “Improvement of sound source localization in a finite duct using beamforming methods,” *Applied acoustics,* vol. 103 , no. 37-46, 2016.

[11] K. Gao, H. Kuai, S. Huang and W. Jiang, “Localization of broadband acoustical sources in the cylindrical duct via measurements outside the duct end.,” *Journal of Sound and Vibration,* vol. 562, no. 117749, 2023.

[12] X. Wang and M. S. Ghidaoui, “Identification of multiple leaks in pipeline: Linearized model, maximum likelihood, and super-resolution localization,” *Mechanical Systems and Signal Processing,* vol. 107 , pp. 529-548, 2018.

[13] Z. Hu, S. Tariq and T. Zayed, “A comprehensive review of acoustic based leak localization method in pressurized pipelines.,” *Mechanical systems and signal processing,* vol. 161 , p. 107994, 2021.

[14] R. Worley, Y. Yu and S. Anderson, “Acoustic Echo-Localization for Pipe Inspection Robots,” in *2020 IEEE International Conference on Multisensor Fusion and Integration for Intelligent Systems (MFI)*, 2020.

[15] L. Jing, Z. Li, Y. Li and R. D. Murch, “Channel characterization of acoustic waveguides consisting of straight gas and water pipelines,” *IEEE Access ,* vol. 6, pp. 6807-6819, 2018.

[16] L. Jing, M. Wang, Y. Lu, M. Stojanovic and R. Murch, “Differential orthogonal frequency division multiplexing communication in water pipeline channels,” *The Journal of the Acoustical Society of America,* vol. 148, no. 2, pp. EL130-EL134, 2020.

[17] Z. Li, Y. Yu and K. V. Horoshenkov, “A comparison of the performance of four acoustic modulation techniques for robot communication in pipes.,” *The International Journal of Acoustics and Vibration,* vol. 28, no. 1, pp. 98-116, 2023.

[18] P. M. Morse and K. U. Ingard, Theoretical acoustics, Princeton university press, 1986.

[19] Y. Yu, A. Krynkin, Z. Li and K. V. Horoshenkov, “Analytical and empirical models for the acoustic dispersion relations in partially filled water pipes,” *Applied Acoustics,* vol. 179, no. 0003-682X, p. 108076, 2021.

[20] Y. Yu, A. Krynkin and K. V. Horoshenkov, “The effect of 3D surface roughness on acoustic wave propagation in a cylindrical waveguide.,” *Wave Motion,* p. 103304, 2024.

[21] S. L. Brunton and J. N. Kutz., Data-driven science and engineering: Machine learning, dynamical systems, and control., Cambridge University Press, , 2019..

[22] S. J. Wright, R. D. Nowak and M. A. Figueiredo, "Sparse reconstruction by separable approximation," *IEEE Transactions on Signal Processing,* vol. 57(7), pp. 2479-2493, 2009.

[23] S. V. Vaseghi, Advanced digital signal processing and noise reduction, John Wiley & Sons, 2008.

[24] C. C. Paige and M. A. Saunders, "LSQR: An algorithm for sparse linear equations and sparse least squares.," *ACM Transactions on Mathematical Software (TOMS),* vol. 8, no. 1, pp. 43-71, 1982.

1

2